

Full paper

A conditioning circuit with exponential enhancement of output energy for triboelectric nanogenerator

Ali Ghaffarinejad^{a,b}, Javad Yavand Hasani^{b,*}, Ronan Hinchet^c, Yingxian Lu^a, Hemin Zhang^a, Armine Karami^d, Dimitri Galayko^d, Sang-Woo Kim^c, Philippe Basset^{a,*}

^a Université Paris-Est, ESYCOM, ESIEE Paris-CNAM-UPEM, Noisy-le-Grand 93162, France

^b School of Electrical Engineering, Iran University of Science and Technology, Tehran 16846-13114, Iran

^c School of Advanced Materials Science and Engineering, Sungkyunkwan University (SKKU), Suwon 440-746, Republic of Korea

^d Sorbonne Universités, F-75005 Paris, France

ARTICLE INFO

Keywords:

Triboelectric-electret (triboelectret) nanogenerator
Bennet's doubler
Power management circuit
Conditioning circuit
Kinetic energy harvester
T-ENG

ABSTRACT

Triboelectric-electret nanogenerators (T-ENG) are characterized by their high output voltage and small current and therefore a relatively low output power, making them limited to small power consuming electronics. Here we report a self-enhancing conditioning circuit (CC) that exponentially amplifies the output electrical energy converted from the mechanical domain of a T-ENG, in orders of magnitude compared to traditional CC. The circuit, working on the principles of Bennet's doubler device, is inductorless and uses only diodes as automatic switches to reconfigure the charge storing capacitors between series and parallel modes. We previously reported this circuit in saturation and stable mode for T-ENG and compared the performances with half-wave rectifier. Here we investigate the circuit performance in exponential and unstable mode in comparison with half-wave and full-wave rectifiers. Theoretical analysis is presented to study the operation of the circuit and to find out the required conditions for the Bennet's doubler to work in exponential boosting mode. Output performance of half and full wave rectifiers are compared theoretically. Simulations and experiments are performed to verify the theoretical discussions and to present the effect of non-ideal circuit elements on the output performance of the T-ENG.

1. Introduction

With the development of Internet of things (IOT) and portable devices, a vast variety of small electronic instruments are becoming parts of our daily life. Powering such devices is a challenge that is to be overcome, either by using rechargeable batteries or harvesting electrical energy from ambient energy. Electrostatic kinetic energy harvesters (e-KEH) convert the kinetic energy of mechanical vibrations into electrical energy by varying the capacitance of an electromechanical transducer [1]. These transducers require an initial bias to work properly, which is provided either by an external power source [2], an electret layer embedded in the variable capacitor of the device [3,4] or a triboelectric contact between the capacitor's electrodes [5]. Although electrets are preferable to a battery, they can lose charge over the time and render the harvester useless. Triboelectric charge generation can be a solution to this problem, since successive contacts continuously accumulate triboelectric charge on the surface of dielectric materials [5]. Such e-KEH are called Triboelectric-Electret Nano Generator (T-ENG)

[6], and the initial bias comes from the charge transfer between the materials covering the electrodes of the harvester with different electronegativity conditions.

T-ENG is a promising technology to provide the power for small electronic tools, however there are still several challenges on the way to practical applications. Unlike non-contact electret-based e-KEHs, tribo-based e-KEHs do not carry a pre-imposed charge and the surface density of tribo-charges depends on many parameters like contact force, humidity, coefficient of friction, surface energy, surface roughness or electron affinity of the contacting surfaces [7–10]. Thus, the generated charges are not uniformly distributed on the surface and the charge density changes from one point to another point. Due to the nature of triboelectric contact and charge generation, the tribo-charge density hardly reaches the theoretical maximum as with corona-charged electret [11]. As a result, e-KEH's that rely only on triboelectricity usually produce less energy per cycle compared to other electret-based e-KEH's. Therefore, the biggest challenge is to manage the relatively small quantity of charges produced by T-ENG in a way that increases the total

* Corresponding author.

E-mail addresses: yavand@iust.ac.ir (J.Y. Hasani), philippe.basset@esiee.fr (P. Basset).

efficiency of the electromechanical transducer. Various conditioning circuits (CC) and configurations have already been introduced to enhance the total power produced by T-ENG's. In [12], Thang et al. and Zi et al. in [13] used a combination of serial and parallel mechanical switches to improve the output power of the T-ENG. In [14], Zhu et al. directly attached a transformer to the triboelectric harvester to enhance the power. In [15], Niu et al. implemented a two stage logically-controlled switching system in combination with coupled inductors to increase the power transfer efficiency. In [16], Xi et al. used a MOSFET switch controlled by a comparator to manage the charge flow from the T-ENG. Cheng et al. in [17] investigated a new approach by connecting the electrodes of the T-ENG to the ground through different switching modes. In [18], Cheng et al. developed a two-step process for delivering the energy to a load with series-switches and LC transformers. In [19] Niu et al. succeeded in a time domain analysis of a TENG managed by a full-wave rectifier. They optimized the output performance of a contact-separation mode TENG by calculating the optimum capacitance load for the maximum energy storage based on the characteristics of the TENG. They also derived the charging time constant for the capacitive load. Zi et al. in [20] designed an innovative charging cycle for a TENG conditioned by a full-wave rectifier. By adding a mechanical switch connected in parallel with the TENG they improved the maximum energy-storage efficiency by 50%.

In this paper, we introduce the Bennet's charge doubler as a new CC for T-ENG that only uses diodes and capacitors. No mechanical switch or external control is required to store the harvested energy in a reservoir capacitor. The main characteristic of this circuit is its ability to exponentially increase the voltage across the reservoir capacitance. In recent years, the attractiveness of the Bennet's doubler and related circuits for e-KEH is increasing [21–23]. Previously, we investigated the power boosting features of the Bennet's charge doubler for T-ENG in the saturation mode [24]. Here, for the first time, we demonstrate the application of the exponential mode for T-ENG's.

2. Theoretical analysis

2.1. Modeling of the T-ENG

The physics of tribo-charge generation and storage due to repeated contacts is still under study and a full insight into the process is missing [25,26]. From the operational point of view, A T-ENG belongs to the same family as electret-based kinetic energy harvester's [6] that has been under study for years [27–29]. The structure of the contact-mode triboelectric energy harvester used in this study is shown in (Fig. 1). The transducer is a variable parallel plate capacitor with two electrodes of aluminum and two stacking layers of dielectrics; a 50 μm -PFA layer and a double side tape to stick it to the fixed electrode. The top electrode is forced by a magnetic shaker to move in the vertical direction and make repeated contacts with the top dielectric layer, and generates triboelectric charges. The contact

force is measured by a force sensor. The generated surface triboelectric charges Q_{TE} are stored on the surface of PFA and induced charges on the top and bottom electrodes (Q_{var} and Q_{die} respectively) that vary with the T-ENG's capacitance variation. It is assumed that the stored triboelectric charges on the surface of PFA are accumulated in energy traps very close to the surface layer [30]. To simulate the characteristic of the Bennet's doubler, we adopted the lumped model presented by Hinchet et al. in [6] for representing the triboelectric harvester.

Using the Gauss law for the electrostatics of the structure we have:

$$E_{PFA}\epsilon_{PFA} + E_{var}\epsilon_{air} = -Q_{TE}/(\epsilon_0 S) \quad (1)$$

$$S\epsilon_0\epsilon_{air}E_{var} - Q_{var} = 0 \quad (2)$$

$$S\epsilon_0\epsilon_{tape}E_{tape} - Q_{die} = 0 \quad (3)$$

where ϵ_{air} , ϵ_{PFA} and ϵ_{tape} are the relative permittivity of the air, PFA layer and adhesive tape respectively, and ϵ_0 is the permittivity of the vacuum. E_{var} , E_{PFA} and E_{tape} are the electric fields in the air gap, the PFA layer and in the adhesive tape, respectively. Charge conservation principle requires the following relation between Q_{var} , Q_{die} and Q_{TE} :

$$Q_{TE} + Q_{var} + Q_{die} = 0 \quad (4)$$

Using the Poisson's equation for the three charge distributions we find that:

$$\begin{aligned} V_{T-ENG} = & - \int_0^{d_{tape}} E_{tape} dx - \int_{d_{tape}}^{d_{tape}+d_{PFA}} E_{die} dx \\ & + \int_{d_{tape}+d_{PFA}}^{d_{tape}+d_{PFA}+d_{var}} E_{var} dx = -E_{tape}d_{tape} - E_{PFA}d_{PFA} \\ & + E_{var}d_{var} \end{aligned} \quad (5)$$

after putting Eqs. (1–4) into Eq. (5), we get:

$$V_{T-ENG} = \frac{Q_{TE}}{S\epsilon_0} \left(\frac{d_{PFA}}{\epsilon_{PFA}} + \frac{d_{tape}}{\epsilon_{tape}} \right) + \frac{Q_{var}}{S\epsilon_0} \left(\frac{d_{PFA}}{\epsilon_{PFA}} + \frac{d_{tape}}{\epsilon_{tape}} + \frac{d_{var}}{\epsilon_{air}} \right) \quad (6)$$

A full proof for Eq. (6) is presented in section S1. Eq. (6) can be further simplified by the following definitions:

$$C_{T-ENG} = \epsilon_0 S \frac{1}{\frac{d_{PFA}}{\epsilon_{PFA}} + \frac{d_{tape}}{\epsilon_{tape}} + \frac{d_{var}}{\epsilon_{air}}} \quad (7)$$

$$C_{die} = \epsilon_0 S \frac{1}{\frac{d_{PFA}}{\epsilon_{PFA}} + \frac{d_{tape}}{\epsilon_{tape}}} \quad (8)$$

$$V_{TE} = \frac{Q_{TE}}{C_{die}} \quad (9)$$

where V_{TE} is a constant voltage, C_{die} is the total capacitance of the two dielectric layers with effective thickness of $d_{die} = d_{PFA}/\epsilon_{PFA} + d_{tape}/\epsilon_{tape}$ and C_{T-ENG} is the total variable capacitance of the T-ENG. Finally, the T-

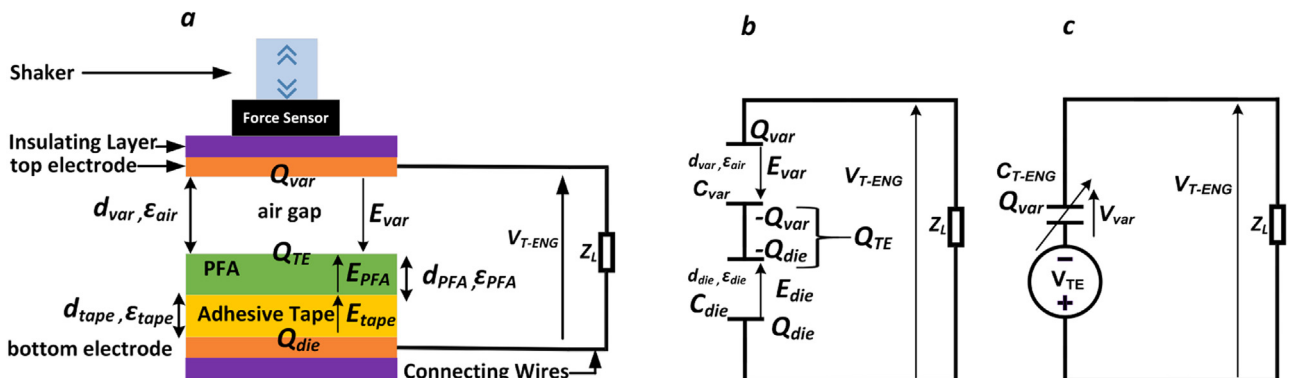


Fig. 1. a. Structure of the T-ENG used in the experiments. b. Detailed and c. lumped models of the T-ENG used in the equations (from [6]).

ENG is modeled by the following formula and the lumped elements shown in (Fig. 1c) [6]:

$$V_{T-ENG} = -V_{TE} + \frac{Q_{var}}{C_{T-ENG}} \quad (10)$$

With a periodic excitation of the top electrode by the shaker, the gap distance of d_{var} changes between a maximum and minimum value and the total variable capacitance of the device C_{T-ENG} (Eq. (7)) will change between a maximum and minimum value as $C_{min} \leq C_{T-ENG} \leq C_{max}$. This allows to define a very important characteristic parameter of the harvester denoted as “capacitance ratio”:

$$\eta = C_{max}/C_{min} \quad (11)$$

2.2. Theoretical development of Bennet’s doubler conditioning circuit

The concept of a machine or a doubler of electricity capable of detecting minute quantities of electrical charges was first discussed by Bennet *et al.* [31]. They devised an instrument made of three conducting plates that increases the amount of stored charges on the plates at each cycle of operation. Queiroz in [32] reinvented the idea by replacing the mechanical contacts by diodes acting as automatic switches. The theory of Bennet’s doubler as a conditioning circuit for electrostatic kinetic energy harvester (e-KEH) is investigated in [33]. We previously introduced the first application of Bennet’s conditioning circuit for the T-ENG in stable mode of operation and compared the performances with the half-wave rectifier [34]. Here we present the thorough theoretical analysis of the circuit in its unstable mode.

Bennet’s doubler belongs to a family of conditioning circuits that implements a rectangular QV cycle [35]. The simplest form of a Bennet’s doubler circuit, its QV diagram in i^{th} cycle of the operation and the state of diodes during this cycle are shown in (Fig. 2). The objective of the analysis in this section is to find the dynamic evolution of charges and voltages on the three capacitors C_{store} , C_{res} and C_{T-ENG} during one cycle, and to derive the required conditions of the T-ENG for the Bennet circuit to work in exponential (unstable) mode. For the simplicity of the

demonstration, we use the following assumptions not restraining the generality of the study: (i) the fixed capacitors are equal ($C_{store} = C_{res} = C$) and (ii) ideal characteristics are considered for the diodes, which means zero voltage drop in forward bias and zero leakage current in reverse bias.

At point A of the QV diagram in Fig. 2b, where $C_{T-ENG} = C_{max}$, the voltages V_{st} , V_{res} and V_{T-ENG} are denoted as V_{st_i} , V_{res_i} and V_{T-ENG_i} ; also at point D where $C_{T-ENG} = C_{min}$, the voltages are denoted as V_{st_i} , V_{res_i} and V_{T-ENG_i} . Dynamic analysis starts at the beginning of the i^{th} cycle when $C_{T-ENG} = C_{max}$ and the voltages of all three capacitors are equal to the same value as follow:

$$V_{st_i} = V_{res_i} = V_{T-ENG_i} = V_i \quad (12)$$

Starting from point A and moving toward point B, C_{T-ENG} decreases from C_{max} and V_{T-ENG} start to increase above V_i . All the diodes are off as long as $V_{T-ENG} < 2V_i$ and the transducers charge remain constant at value of point A which is $Q = C_{max}(V_i + V_{TE})$. At point B, where $C_{T-ENG} = 2C_{min}$ [1] we have $V_{T-ENG} = 2V_i$, D_2 turns on and C_{store} and C_{res} are connected in series as in Fig. 2c. Moving from B to D, the harvester gives a certain amount of charge (generated charge) to the series combination of C_{store} and C_{res} , which we denote by ΔQ_{gi} . The generated charge by transducer at the i^{th} cycle is written as:

$$\Delta Q_{gi} = (V_i + V_{TE})C_{max} - (V_{T-ENG_i} + V_{TE})C_{min} \quad (13)$$

where the V_{T-ENG_i} is the transducer voltage (also the voltage on the series combination of C_{store} and C_{res}) at point D. This voltage can be found by employing charge conservation law between the two points of B and D (section S6) and finally the given charge to C_{store} and C_{res} is figured out as:

$$\Delta Q_{gi} = V_i \frac{C_{max} - 2C_{min}}{\frac{C}{2} + C_{min}} + V_{TE} \left(\frac{(C_{max} - C_{min})C_{min}}{\frac{C}{2} + C_{min}} + C_{max} - C_{min} \right) \quad (14)$$

It is imperative to understand that ΔQ_{gi} is the amount of charge given by transducer to each of the capacitors C_{store} and C_{res} . So, from C_T

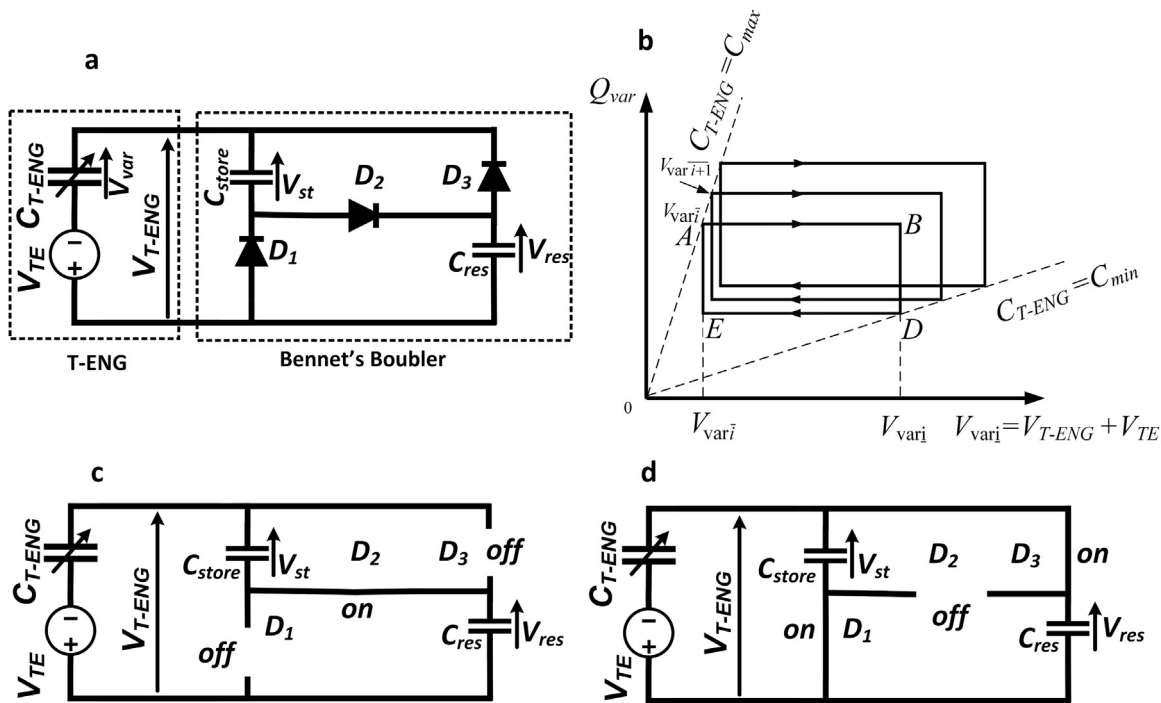


Fig. 2. a. Typical connection of the T-ENG to the Bennet’s doubler circuit to store the output energy in C_{res} . b. QV diagram of the T-ENG with Bennet’s doubler in steady-state. c. State of diodes in the B→D section of the QV diagram when charge storing capacitances of C_{store} and C_{res} are in series connection. d. State of diodes in the E→A section of the QV diagram when charge storing capacitances of C_{store} and C_{res} are in parallel connection.

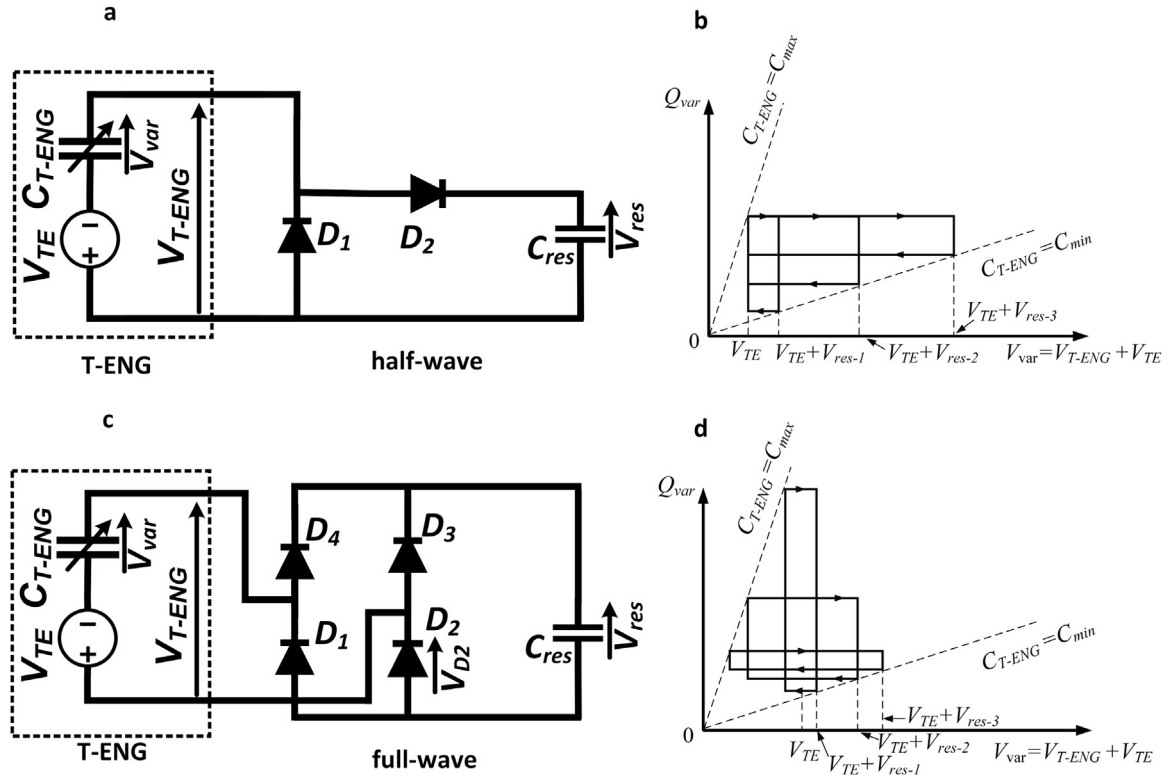


Fig. 3. Basic diode bridges as conditioning circuits for T-ENG for the purpose of storing the converted energy in reservoir capacitance of C_{res} and corresponding charge-voltage diagrams. a and b. Half-wave. c and d. Full-wave. The two QV diagrams are plotted with assumption of $C_{res} \gg C_{max}$.

$ENG = C_{max}$ to $C_{T-ENG} = C_{min}$ the total charge of the system of three capacitors changes as:

$$-\Delta Q_{gi} + \Delta Q_{gi} + \Delta Q_{gi} = \Delta Q_{gi} \quad (15)$$

As C_{T-ENG} starts increasing from C_{min} at point D, the voltage of V_{T-ENG} decreases and D_2 turns off. The harvester keeps its charge until $V_{T-ENG} = V_{var} - V_{TE}$ drops below $V_{sl_i} = V_{res_i}$ at point E and D_1 and D_3 turns on simultaneously and C_{store} , C_{res} and C_{T-ENG} reconfigure in the parallel mode as in Fig. 2d. Employing similar analysis as above, the charge given to C_{T-ENG} from point E to A by the parallel combination of C_{store} and C_{res} is ΔQ_{gi} , which means $\Delta Q_{gi}/2$ is reduced from each of them. As a result, it is observed that during a complete cycle of operation each of the capacitors C_{store} , and C_{res} gain $\Delta Q_{gi} - \Delta Q_{gi}/2 = \Delta Q_{gi}/2$ amount of charge.

To derive the total charge and the voltage V_{i+1} at the beginning of the $i^{th} + 1$ cycle, the charge ΔQ_{gi} must be added to the total charges that the capacitors had at the beginning of the i^{th} cycle. Therefore, the charge balance equation is derived as follow:

$$V_{i+1}(2C + C_{max}) = V_i(2C + C_{max}) + \Delta Q_{gi} \quad (16)$$

where $2C$ is the equivalent of the two parallel capacitors. By substitution of Eq. (14) into the last expression we get:

$$V_{i+1} = V_i \left[1 + \frac{C_{max} - 2C_{min}}{2C + C_{max}} \times \frac{C/2}{C_{min} + C/2} \right] + V_{TE} \left(\frac{C_{max} - C_{min}}{2C + C_{max}} \right) \left(1 + \frac{C_{min}}{C_{min} + C/2} \right) \quad (17)$$

Formula 16 indicates that at the beginning of $i^{th} + 1$ cycle the total charge of the capacitors is higher than that of the total charge at beginning of the i^{th} cycle. It also states that $i^{th} + 1$ cycle starts with a slightly higher voltage V_{i+1} . This increase is exponential if the coefficient multiplied by V_i in Eq. (17) is larger than one, which means $C_{max} > 2C_{min}$. Otherwise, when $C_{max} < 2C_{min}$ the voltage across all the

capacitors would saturate after a certain amount of time depending to the time constant of the circuit. Therefore, for $\eta > 2$ the Bennet's doubler works in exponential mode, while, for $\eta < 2$, the Bennet doubler works in the saturation mode. The total energy delivered to the network of the three capacitors is the sum of energy gained by each capacitors in one cycle as follow:

$$\Delta W_i = \frac{1}{2} [C_{max} ((V_{i+1} + V_{TE})^2 - (V_i + V_{TE})^2) + 2C (V_{i+1}^2 - V_i^2)] \quad (18)$$

The converted energy is distributed across the capacitors C_{max} , C_{res} , C_{store} . For practical applications we should defined $C_{max} < C_{store} < C_{res}$ so that most of the gained energy is stored in the reservoir capacitor C_{res} . By respecting this definition and merging Eq. (17) with 18 we have (section S7):

$$\Delta W_i = V_i^2 (C_{max} - 2C_{min}) \left(1 + \frac{C_{max}}{2C} \right) + V_i V_{TE} \left(C_{max} - C_{min} + C_{max} \frac{2C_{max} - 3C_{min}}{2C} \right) + V_{TE}^2 \left(C_{max} \frac{C_{max} - C_{min}}{2C} \right), \quad (19)$$

which is defined as stored energy in C_{res} in the i^{th} cycle of operation of the T-ENG.

Although the exponential performance of the original Bennet's doubler is limited to the capacitance ratios above 2, there are specific configurations that work in the exponential mode with ratios below 2 [33,36]. However, for the T-ENG's with capacitance ratio of 1, the Bennet's doubler does not work in the exponential mode [37,38].

2.3. Charge-voltage evolution in half and full wave diode rectifiers

From analytical point of view, electrical evolution of full-wave and half-wave rectifiers in combination with a T-ENG follows a rectangular QV diagram [35,39]. Fig. 3a and c shows typical connection of T-ENG

with the half and full wave rectifiers respectively. Fig. 3b and d indicates typical QV diagrams of full and half wave rectifiers [1]. Theoretical development of diode states and charging of C_{res} is similar to the formulation performed for the Bennet's doubler [1].

2.3.1. Half-wave conditioning circuit

For the case of the half-wave rectifier with the assumption of $C_{res} \gg C_{max}$, the converted energy in i^{th} cycle of operation is formulated as [1] (Section S8):

$$\Delta W_{i_HW} = V_{TE} V_{res-i} C_{max} \left(1 - \frac{1 + V_{res-i}/V_{TE}}{\eta} \right) \quad (20)$$

where η is the capacitance ratio defined with Eq. (11) and V_{res-i} is the voltage across the reservoir capacitance of C_{res} at the i^{th} cycle. The energy ΔW is a quadratic function of V_{res} ; therefore, there is an optimal value for V_{res} that the converted energy is maximum as long as V_{TE} , C_{max} and C_{min} are constant which is found as:

$$V_{res_HW}(\text{opt}) = \frac{1}{2} V_{TE} (\eta - 1) \quad (21)$$

The $V_{res_HW}(\text{opt})$ is found by taking the derivative of ΔW_{i_HW} with respect to V_{res-i} from Eq. (20) and equating to zero. The maximum energy delivered by the half-wave rectifier is then equal to:

$$\Delta W_{max_HW} = \frac{1}{4} V_{TE}^2 C_{min} (\eta - 1)^2 \quad (22)$$

2.3.2. Full-wave conditioning circuit

For the full wave rectifier as shown in Fig. 3c, also with the assumption of $C_{res} \gg C_{max}$, the converted energy in i^{th} cycle is [1] (section S8):

$$\Delta W_{i_FW} = 2V_{res-i} C_{min} (\eta + 1) \left(V_{TE} \frac{\eta - 1}{\eta + 1} - V_{res-i} \right) \quad (23)$$

the optimum value of reservoir voltage for the maximum delivered energy is:

$$V_{res_FW}(\text{opt}) = \frac{1}{2} V_{TE} \left(\frac{\eta - 1}{\eta + 1} \right) \quad (24)$$

Therefore, the maximum converted energy is given by:

$$\Delta W_{max_FW} = \frac{1}{2} V_{TE}^2 C_{min} \frac{(\eta - 1)^2}{(\eta + 1)} \quad (25)$$

By dividing the maximum energy of the two bridge circuit we have [40]:

$$\frac{\Delta W_{max_HW}}{\Delta W_{max_FW}} = \frac{1}{2} (\eta + 1) \quad (26)$$

Since in practice $\eta > 1$, this formula exhibit the fact that half-wave rectifier always converts a higher maximum energy compared to the full-wave rectifier.

3. Experimental results and simulation analysis

3.1. T-ENG and experimental setup descriptions

In this study, we used three T-ENG's, with contact area of $3 \times 3 \text{ cm}^2$, $5 \times 5 \text{ cm}^2$ and $10 \times 10 \text{ cm}^2$. They all work in contact-release mode and electric charge is generated on the dielectric surface by contact electrification, which induces positive charge on the metal electrodes by the principle of electrostatic induction. As shown in Fig. 1, they are made of two aluminum electrodes. A double sided adhesive tape with thickness of $80 \mu\text{m}$ and relative permittivity of 3 is attached onto the bottom electrode to hold the $50 \mu\text{m}$ PerFluoroAlkoxy (PFA) polymer. The

polymer is provided by GoodFellow [41] with a permittivity of 2.1. The top electrode is isolated by an additional insulator and attached to the force sensor, which in turn is attached to a magnetic shaker. The shaker provides a vertical sinusoidal motion of the top electrode with a frequency of 5 Hz.

3.2. Characterization of the T-ENG

3.2.1. Dynamic T-ENG capacitance

The time variation of the transducer's capacitance C_{T-ENG} can be measured using the technique described in [6,42]. From the measurement, C_{max} , C_{min} and η are derived. The proper setup for this technique and the details of the method are reminded in the supplementary material (section S2 and Fig. S1). Typical curve of the measured capacitance variation is depicted later for each device.

3.2.2. T-ENG surface voltage

For the purpose of simulations, V_{TE} can be found using the configuration presented in Fig. 3a and the following formula [1] :

$$V_{TE} = \frac{V_{res}(\text{sat})}{C_{max}/C_{min} - 1} \quad (27)$$

where $V_{res}(\text{sat})$ is the measured saturation value of V_{res} obtained from the setup.

3.3. Performance comparison between conditioning circuits

From Fig. 2a, as the triboelectric energy harvester starts, the voltage across the reservoir capacitor C_{res} starts to build up exponentially under conditions discussed in Section 2.2. To investigate the efficiency of the Bennet's doubler as a CC for the T-ENG's, we compared the output characteristics of the Bennet circuit with that of half-wave and full-wave rectifier circuits (Fig. 3a and c). Fixed capacitance values are selected as $C_{res} = 4.7 \text{ nF}$ and $C_{store} = 100 \text{ nF}$. The diodes used in the circuits are commercially available 1n649 (Microsemi) with 835 V of measured breakdown voltage. The overlapping area of the electrodes is $10 \times 10 \text{ cm}^2$ and the maximum applied force on the surface of the polymer at the contact is $F = 1.33 \text{ N}$. Fig. 4a shows the measured capacitance variation of the device with the technique introduced in section S2. The maximum and minimum peaks of the curve are 708 and 160 pF respectively. After reduction of the 16 pF of shunt parasitic capacitance, $C_{max} = 692 \text{ pF}$ and $C_{min} = 144 \text{ pF}$, corresponding to a ratio of $\eta = 4.8$. Fig. 4b shows the charging curves of V_{res} across the capacitance C_{res} for all three CC. Half-wave and full-wave rectifiers quickly charge the reservoir capacitance C_{res} to a moderate saturation value, 165 V and 26 V respectively, but the Bennet's doubler performance rises up to 835 V after 140 s Fig. 4c indicates the measurement of the energy per cycle per time of the stored charges in C_{res} . The insets show that the full-wave rectifier indicates a better performance for the first five seconds, and the half-wave for the first 32.6 s. After these, the harvester's operation of the converted energy per cycle stored in C_{res} by the Bennet doubler starts to outperform that of diode bridges. Fig. 4d shows the delivered energy at each cycle as a function of the voltage across the reservoir capacitance C_{res} . From the inset figure, it can be viewed that the delivered energy of the Bennet's circuit overcomes the one of the half-wave bridge for output voltages above 127 V. For a low voltage load with $V_{res} = 3 \text{ V}$ the harvested DC power is 21.5 nW, 350 nW and 455 nW for Bennet, half-wave and full-wave respectively. To handle the high output voltage of the Bennet's doubler and make it suitable for low voltage electronics such as RFID's or implantable biomedical devices several architectures can be implemented. A simple concepts which use direct switching of the output voltage and storing the energy into a storage capacitor that derives the load is suggested in [33,43]. More comprehensive approaches which employ flyback converters or step-down DC-DC Buck converters are discussed in [44–48].

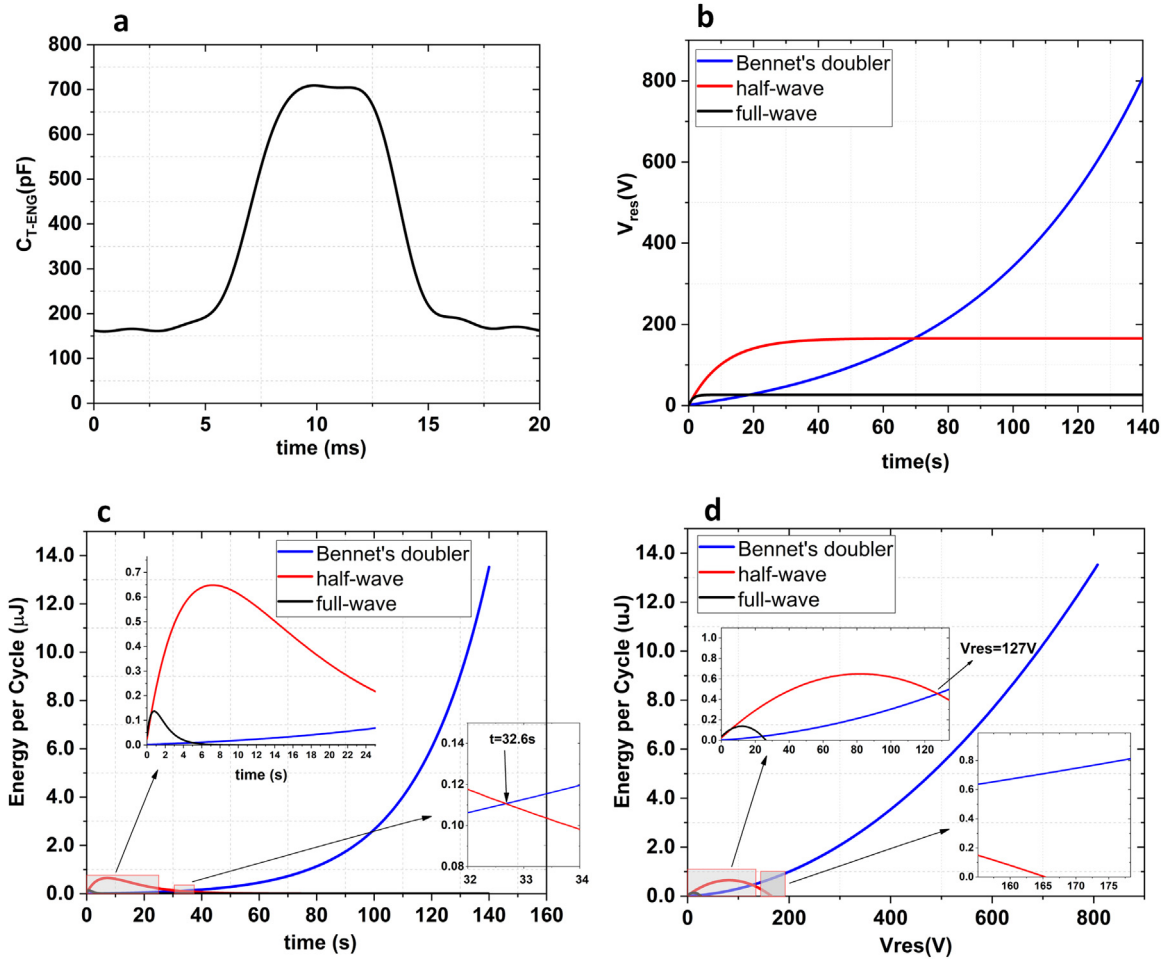


Fig. 4. Experimental comparison of the output characteristics of the half and full-wave rectifiers with Bennet’s doubler for the $10 \times 10 \text{ cm}^2$ device with contact force of 1.33 N. a. Variation of C_{T-ENG} in one cycle of operation measured by technique introduced in Section 3.2. b. Charging curves across C_{res} for the three conditioning circuits. c. Stored energy per each cycle in C_{res} for the three conditioning circuits. d. Stored energy in C_{res} as a function of V_{res} .

3.4. Simulation and comparison of the three conditioning circuits

3.4.1. Model parameter extraction

Using measurements of C_{T-ENG} and V_{TE} , we performed lumped-model simulations in LTspice of the three CC to have a deeper understanding of their performances. The variation of air gap d_{var} is approximated as a sinusoidal function with the following formula:

$$d_{var} = d_{min} + \frac{d_{max} - d_{min}}{2} [\sin(2\pi ft) + 1] \quad (28)$$

where d_{min} and d_{max} are minimum and maximum gap between the top electrode and PFA surface, corresponding to C_{max} and C_{min} respectively with respect to Eq. (7). Simulation parameters for the $10 \times 10 \text{ cm}^2$ device are given in Table 1.

It should be noticed that the measured value of C_{max} is smaller than the value of C_{T-ENG} obtained from the Eq. (7) by setting $d_{min} = 0$. Eq. (7) gives 1.75 nF, while C_{T-ENG} at rest and when a light constant force of

Table 1

Parameters for lumped model simulation of the $10 \times 10 \text{ cm}^2$ and $5 \times 5 \text{ cm}^2$ T-ENG.

	5×5	10×10
Area (cm^2)	5×5	10×10
Frequency f (Hz)	5	
PFA - ϵ_2 / d_2 (μm) (from datasheet)	2.1 / 50	
Adhesive tape - ϵ_3 / d_3 (μm) (from datasheet)	3 / 80	
d_{min} / d_{max} (μm) (from capacitance measurements)	47.4 / 184.8	77.4 / 564
V_{TE} (V) (from Eq. (27))	54.92	43.42

0.12 N is applied gives 660 pF and 673 pF respectively, when measuring it with a RLC impedance meter. This comes from the fact that the interface at the contact is not fully conformal and local free space is trapped between the two colliding surfaces. Previous studies of contact-mode variable capacitive structures also confirm the same outcome [49–52].

3.4.2. Output performance analysis based on QV cycle

As a powerful analytical tool, charge-voltage diagram of a capacitive energy harvester has been used widely to compare and evaluate the output performance of the device [20,53]. Fig. 5 compares simulated QV cycles of the $10 \times 10 \text{ cm}^2$ T-ENG, using data in Table 1, with the Bennet doubler (Fig. 5a), half-wave (Fig. 5b) and full-wave (Fig. 5c) bridges. As mentioned in Section 2.2, the enclosed area defined by the QV curve quantifies the delivered energy by the T-ENG during the corresponding cycle. As expected from Figs. 2 and 3 they all resemble a rectangular QV cycle. The Bennet doubler has an unstable behavior (Fig. 5a), while the two diode bridges have a stable behavior leading to a saturation, which corresponds to a converted energy per cycle close to zero [35,39]. Fig. 5d compares the delivered energy at various cycles between the three circuits, showing again that the diode bridge outperformed the Bennet doubler only at the beginning of the conversion process.

3.5. Comparison of measured and simulated QV cycles

In this section we used a $5 \times 5 \text{ cm}^2$ T-ENG, each diode in the circuit

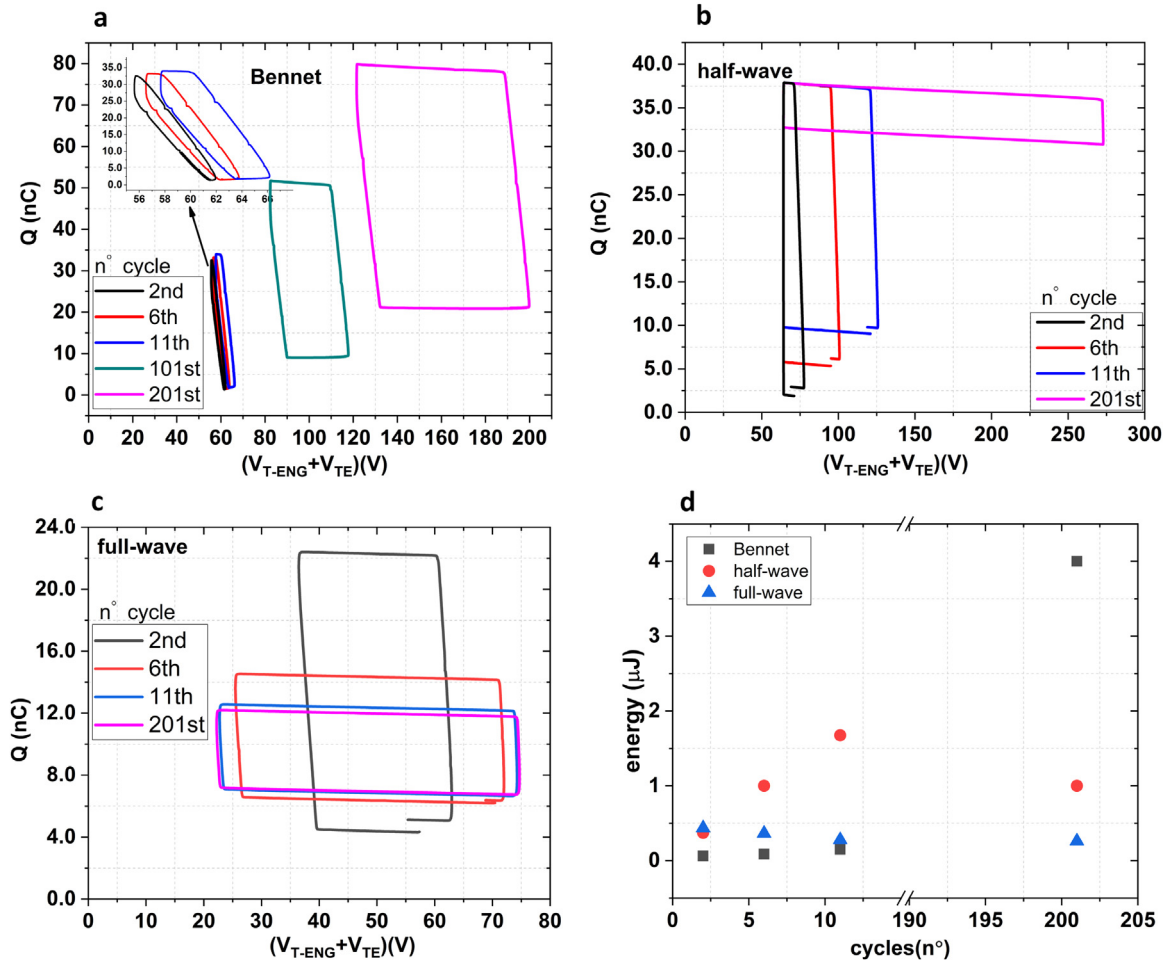


Fig. 5. Comparison of simulated QV cycle of the $10 \times 10 \text{ cm}^2$ T-ENG with the three conditioning circuits. a. Bennet's doubler. b. Half-wave and c. full-wave rectifiers. d. Numerical comparison of energy per cycle extracted from enclosed area of each QV cycle.

is replaced by two low leakage diodes (MMBD1501A provided by FAIRCHILD Semiconductor) with measured breakdown voltage of 280V. The diode model for LTspice simulations is provided by FAIRCHILD (section S5) [54]. $C_{res} = 5 \text{ nF}$ for all three circuits and $C_{store} = 3.3 \text{ nF}$ for the Bennet's doubler. Maximum applied force at the contact of top electrode with PFA surface is measured as 0.2 N with the force sensor. The shaker provides vertical sinusoidal motion of the top electrode at 5 Hz. To measure charge-voltage evolution in time, we measured harvester's current I_{T-ENG} and voltage V_{T-ENG} for the first 30 s. Current measurements is performed with a Keithley 6485 picoammeter. Fig. 6 displays simulated and measured QV curve of the T-ENG with Bennet (Fig. 6a), half wave (Fig. 6b) and full wave (Fig. 6c) rectifiers for the 101st cycle of operation, corresponding to a time interval comprised between 20 and 21 s Fig. 6d and e depict the simulated and measured voltage and current of the T-ENG with Bennet CC respectively. Fig. 6f indicates the charging curve of V_{res} for the half-wave CC with saturation value of $V_{res}(\text{sat}) = 76.9 \text{ V}$. Dynamic capacitance variation of the T-ENG is measured (Fig. S2) using the technique explained in Section 3.2 with extracted values of $C_{max} = 226 \text{ pF}$ and $C_{min} = 94 \text{ pF}$. Thus, Eq. (27) gives the value of $V_{TE} = 54.92 \text{ V}$ which is used for simulating the T-ENG using the lumped model presented by Eq. (10). For the purpose of simulations, values of d_{min} and d_{max} required for Eq. (28) are calculated using the measured values of C_{max} and C_{min} and Eq. (7). (Table S1)

Table 2 indicates extracted energy per cycles from QV cycles of Fig. 6a, b and c. Each measured QV cycle is divided into smaller rectangular to figure out the total enclosed area. To compensate for the mismatch between the start of oscilloscope and picoammeter manual

adjustment is performed in time before calculation of the QV cycle. The loading effect of the measurement setup is the main cause for the reduction in the measured I_{T-ENG} by picoammeter. Typical setup for measuring the QV cycle of the T-ENG is presented is supplementary material (Fig. S3).

4. Bennet's performance under various capacitance variations and non-idealities

4.1. Effect of capacitance ratio on output performance of Bennet's doubler

In this section, we investigate the effect of applied force, capacitance variation and non-ideal diodes on the output performance of the Bennet's doubler. Using the same configuration as in Fig. 1a, a new triboelectric energy harvester is made with polymer area of $3 \times 3 \text{ cm}^2$. Bennet configuration is the same as Fig. 2a with $C_{res} = 4.7 \text{ nF}$ and $C_{store} = 100 \text{ nF}$ and MMBD1501A diodes. By adjusting the motion of the shaker, vertical displacement of the top electrode is controlled and desired values of C_{max} , C_{min} and η are obtained. For each amplitude of the shaker, C_{max} and C_{min} values are measured three times with the technique explained in Section 3.2 to make sure that the process is repeatable. The curves of dynamic variation of capacitances are shown in Fig. S4. Charging curves of V_{res} across C_{res} is recorded for each amplitude of the shaker's movement to compare the output characteristics. The measured maximum contact force for the three tests are 1.33, 0.60 and 0.19 N and the corresponding capacitance ratios are 5.39, 4.38 and 3.52 respectively. Fig. 7a shows the charging curves of C_{res} at 5 Hz for

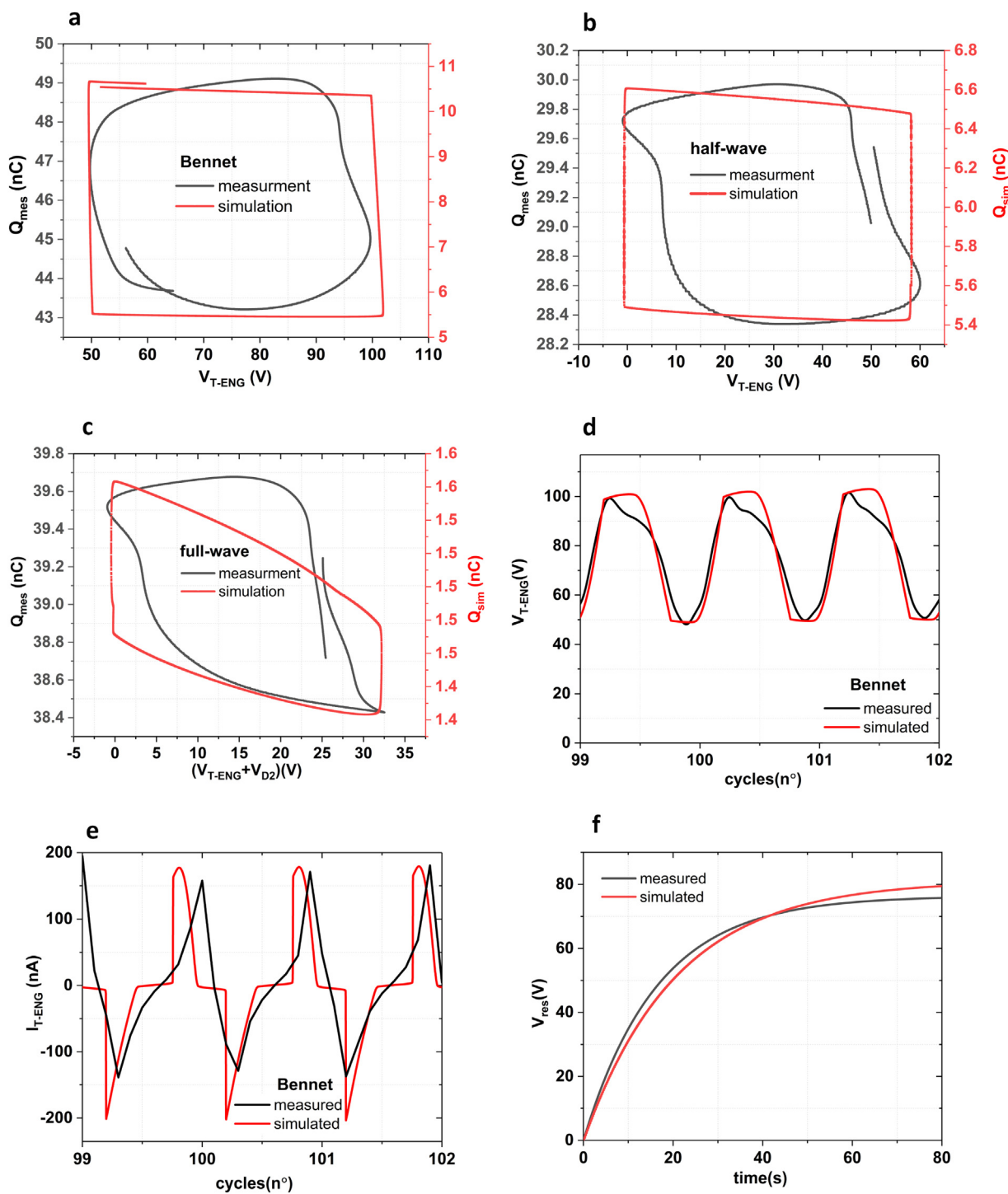


Fig. 6. Measurements and simulations of QV cycle of the T-ENG for the $5 \times 5 \text{ cm}^2$ device at 101st cycle of operation with contact force of 0.2 N. a. Bennet’s doubler. b. Half-wave and c. full-wave conditioning circuits. d and e. Simulated and measured V_{T-ENG} and I_{T-ENG} with Bennet’s doubler. f. Measured and simulated V_{res} for half-wave rectifier used to extract $V_{res}(\text{sat})$ to be used in Eq. (27).

Table 2

Comparison of measured and simulated energy extracted from QV cycle of the T-ENG with Bennet’s doubler, half and full-wave rectifiers. Values extracted from QV curves of Fig. 6.

Energy at 101st cycle (nJ)	Bennet’ doubler	half-wave rectifier	full-wave rectifier
measured	230	61	21
simulated	253	62	27

each value of η . This figure shows that as the applying force and η increase, the charging rate of C_{res} increases too. The charging curves are cut at $V_{res} = 560 \text{ V}$, which is the breakdown voltage of two diodes in series. Fig. 7b indicates C_{max} and C_{min} values as a function of maximum applied force on the PFA surface: C_{max} increases linearly with force while the C_{min} is almost constant. This is understandable since the increase in the contact force removes the trapped air between the top electrode and PFA surface at the contact causing the C_{max} to increase with force. Also, the small decrease of C_{min} as the applied force

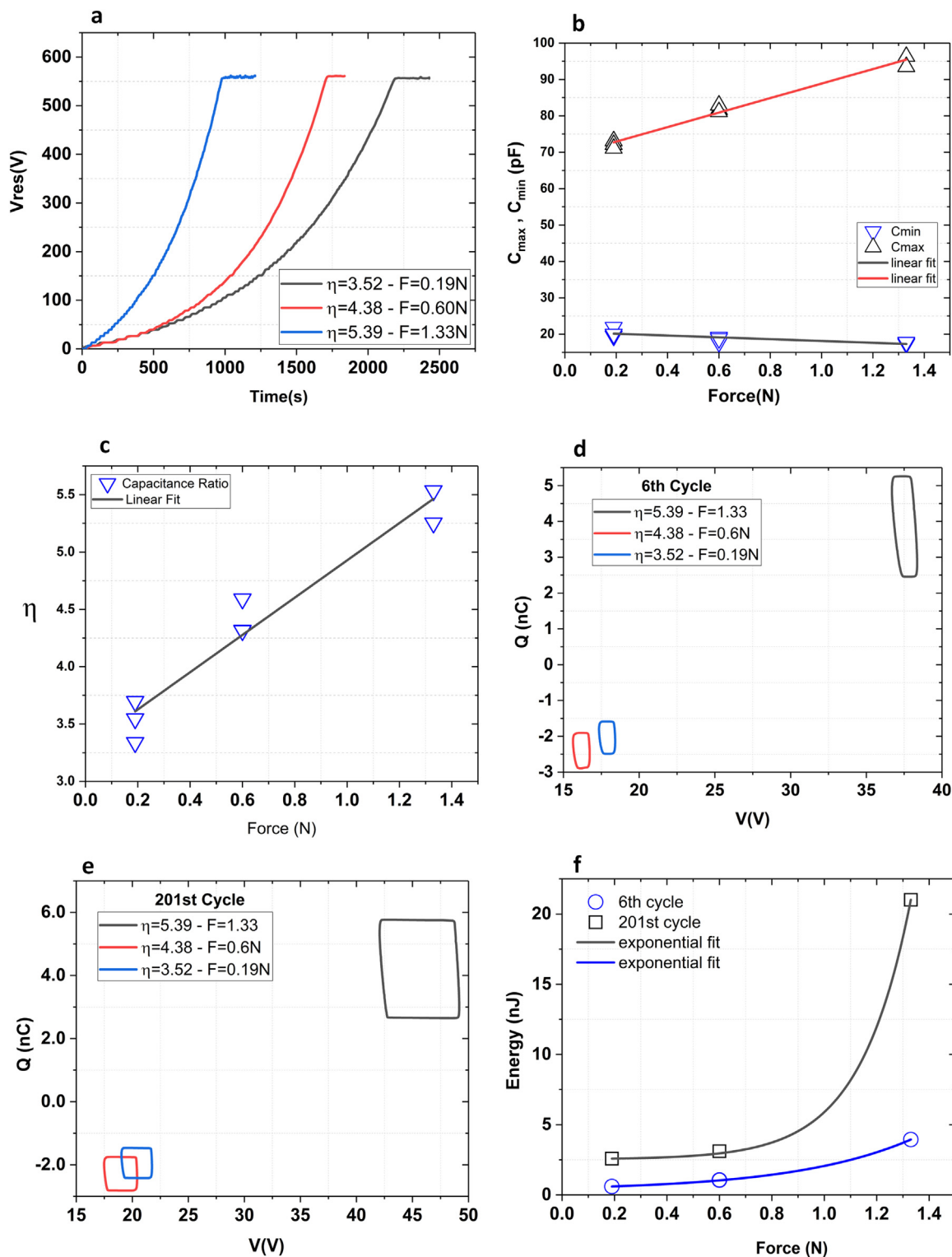


Fig. 7. Effect of capacitance ratio η on output characteristics of the Bennet's doubler for the $3 \times 3 \text{ cm}^2$ device with contact forces of 1.33, 0.6 and 0.19 N. a. Measured charging curves of C_{res} at 5 Hz for three different contact forces. b. Variations of measured C_{max} and C_{min} as a function of applied force. c. Variations of capacitance ratio with applied force. d. Simulated QV cycle of the T-ENG at 6th cycle for increasing η . e. Simulated QV cycle of the T-ENG at 201st cycle for increasing η . f. Force dependency of energy for initial and high cycles of operation. Simulation parameters are included in Table S1.

increases, is due to the motion of the shaker, which increases the maximum distance between the top and bottom electrode. Consequently, Fig. 7c shows the linear dependency of capacitance ratio η to the applied force. Fig. 7d shows the simulated QV diagram corresponding to the 6th cycle of operation of the T-ENG for the three different capacitance ratios. Employed parameters for simulations are

listed in Table S1. The area enclosed in each curve indicates the delivered energy ΔW . Calculation of the enclosed area by rectangle approximation shows that the delivered energy is 0.60 nJ, 1.06 nJ and 3.94 nJ per cycle for $\eta = 3.52, 4.38$ and 5.39 respectively. Fig. 6e indicates simulated QV diagram for the 201st cycle of operation. The delivered energy is 2.58, 3.11 and 21.01 nJ per cycle for $\eta = 3.52, 4.38,$

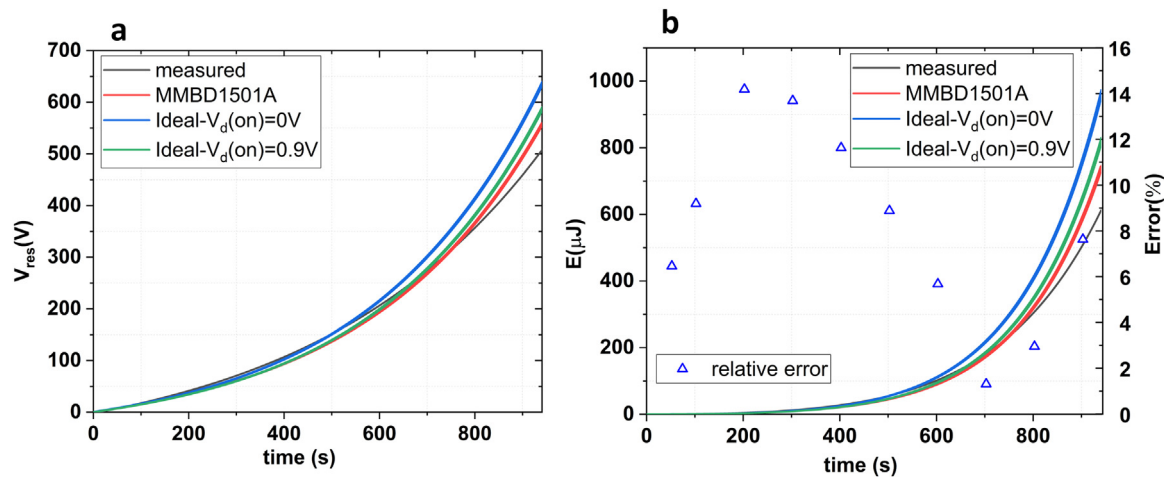


Fig. 8. a. Charging voltage of V_{res} across the capacitance C_{res} , measured, simulated by MMBD1501A diode and two ideal models. b. Total energy stored in the C_{res} for corresponding V_{res} curves and the relative error of employing the diode model. Diode models are presented and discussed in Section S5.

5.39 respectively. Fig. 6f indicates the evolution of the delivered energy per 6th and 201st cycle versus applied force, which shows the strong dependency of the delivered energy at higher cycles of operations to the applied force (and so the capacitance ratio).

4.2. Effect of non-ideality of diodes

The theoretical analysis presented in Section 2 considered the diodes as ideal circuit elements with zero leakage current in reverse bias and zero voltage drop in forward bias. The simulations in Section 3 used the diode model MMBD1501A from Fairchild [54]. To investigate the effect of non-ideal parameters on the output performance of the Bennet's charge doubler, we compared in Fig. 8a the measured output response of V_{res} corresponding to $\eta = 5.39$ with the ones simulated with ideal and MMBD1501A diodes. The two ideal diodes have zero reverse current, 0 V and 0.9 V of turn on voltage V_d (on) in the forward bias respectively. Diode models are discussed in Section S5 and their current-voltage curves are shown in Fig. S5. By comparison, it can be inferred that for the initial cycles of operation, all the simulated curves can trace the measured voltage of V_{res} with a very good approximation; however, for the ending cycles of operation only the curve simulated by the diode model of MMBD1501A shows a good fit.

According to Fig. 8b, the stored energy in C_{res} is also affected if non-idealities are not considered in simulations. The relative error of the simulated curve by the diode model is depicted in Fig. 8b. It can be seen that for almost the whole span of the operation of the T-ENG the relative error is below 9%.

5. Conclusion

In this paper we investigated the performance of a new conditioning circuit based on Bennet's charge doubler in exponential mode in comparison with half-wave and full-wave circuits. This new CC is inductorless with no need for switches or external control. The distributed energy, charge, and voltage across the Bennet's circuit is self-increasing without saturation. The output energy managed by the Bennet's circuit is orders of magnitude higher compared to the other two. By theoretical analysis based on charge-voltage evolution, the dynamics of the Bennet's circuit is studied. By virtue of analytical equations the required conditions for the harvester are found so that the circuit can work in exponential mode. Theoretical comparison of full-wave and half-wave rectifiers are presented. Simulations and measurements of QV diagram confirms better performance of the Bennet's doubler CC. Measured QV cycle of all three CC show an acceptable fit to the curve simulated by the presented model. By experiments the validity of theoretical

outcomes are investigated and the deviation from ideal conditions are discussed. Effect of non-ideal elements on the output performance of the Bennet's doubler is verified through simulations and shows acceptable error for estimation of the performance of the device. With the current trend of switched and externally synced conditioning circuits, it would now be interesting to investigate and compare the performance of the Bennet's doubler with full and half wave rectifiers in controlled-switching mode.

Appendix A. Supplementary material

Supplementary data associated with this article can be found in the online version at <http://dx.doi.org/10.1016/j.nanoen.2018.06.034>.

References

- [1] P. Basset, E. Blokhina, D. Galayko, *Electrostatic kinetic energy harvesting*, Wiley, Hoboken, NJ, 2016.
- [2] Paracha A M, Basset P, Lim P C L, Marty F and Bourouina T, A bulk silicon-based electrostatic vibration-to-electricity energy converter using in-plane-overlap-plate (IPOP) mechanism, in: PowerMEMS'06 Proceedings of the 6th International Workshop Micro Nd N Notechnology Power Gener Tion Nd Energy Convers. Applic Tions Berkeley CA., 2006, pp. 169–172.
- [3] K. Matsumoto, K. Saruwatari, Y. Suzuki, Vibration-powered battery-less sensor node using MEMS electret generator, *Proc. Power MEMS* (2011) 134–137.
- [4] Y. Lu, P. Basset, J.-M. Laheurte, Performance Evaluation of a Long-Range RFID Tag Powered by a Vibration Energy Harvester (1–1), *IEEE Antennas Wirel. Propag. Lett.* (2017), <http://dx.doi.org/10.1109/LAWP.2017.2682419>.
- [5] F.-R. Fan, Z.-Q. Tian, Z. Lin Wang, Flexible triboelectric generator, *Nano Energy* 1 (2012) 328–334, <http://dx.doi.org/10.1016/j.nanoen.2012.01.004>.
- [6] R. Hinchet, A. Ghaffarinejad, Y. Lu, J.Y. Hasani, S.-W. Kim, P. Basset, Understanding and Modeling of Triboelectric-Electret Nanogenerator, *Nano Energy* (2018), <http://dx.doi.org/10.1016/j.nanoen.2018.02.030>.
- [7] E. Németh, V. Albrecht, G. Schubert, F. Simon, Polymer tribo-electric charging: dependence on thermodynamic surface properties and relative humidity, *J. Electrostat.* 58 (2003) 3–16, [http://dx.doi.org/10.1016/S0304-3886\(02\)00137-7](http://dx.doi.org/10.1016/S0304-3886(02)00137-7).
- [8] R. Eilsdon, F.R.G. Mitchell, Contact electrification of polymers, *J. Phys. Appl. Phys.* 9 (1976) 1445–1460, <http://dx.doi.org/10.1088/0022-3727/9/10/010>.
- [9] X. Li, C. Xu, C. Wang, J. Shao, X. Chen, C. Wang, H. Tian, Y. Wang, Q. Yang, L. Wang, B. Lu, Improved triboelectrification effect by bendable and slidable fish-scale-like microstructures, *Nano Energy* 40 (2017) 646–654, <http://dx.doi.org/10.1016/j.nanoen.2017.09.013>.
- [10] D. Kim, S. Lee, Y. Ko, C.H. Kwon, J. Cho, Layer-by-layer assembly-induced triboelectric nanogenerators with high and stable electric outputs in humid environments, *Nano Energy* 44 (2018) 228–239, <http://dx.doi.org/10.1016/j.nanoen.2017.12.001>.
- [11] M.A. Parada, H. Zaias, A. de Almeida, D. Ila, Charge density limits in polymer film electrets, *Charge Density Limits in Polymer Film Electrets*, IEEE, 2005, pp. 304–306, <http://dx.doi.org/10.1109/ISE.2005.1612382>.
- [12] W. Tang, T. Zhou, C. Zhang, F. Ru Fan, C. Bao Han, Z. Lin Wang, A power-transformed-and-managed triboelectric nanogenerator and its applications in a self-powered wireless sensing node, *Nanotechnology* 25 (2014) 225402, <http://dx.doi.org/10.1088/0957-4484/25/22/225402>.
- [13] Y. Zi, H. Guo, J. Wang, Z. Wen, S. Li, C. Hu, Z.L. Wang, An inductor-free auto-

- power-management design built-in triboelectric nanogenerators, *Nano Energy* 31 (2017) 302–310, <http://dx.doi.org/10.1016/j.nanoen.2016.11.025>.
- [14] G. Zhu, J. Chen, T. Zhang, Q. Jing, Z.L. Wang, Radial-arrayed rotary electrification for high performance triboelectric generator, *Nat. Commun.* 5 (2014), <http://dx.doi.org/10.1038/ncomms4426>.
- [15] S. Niu, X. Wang, F. Yi, Y.S. Zhou, Z.L. Wang, A universal self-charging system driven by random biomechanical energy for sustainable operation of mobile electronics, *Nat. Commun.* 6 (2015), <http://dx.doi.org/10.1038/ncomms9975>.
- [16] F. Xi, Y. Pang, W. Li, T. Jiang, L. Zhang, T. Guo, G. Liu, C. Zhang, Z.L. Wang, Universal power management strategy for triboelectric nanogenerator, *Nano Energy* 37 (2017) 168–176, <http://dx.doi.org/10.1016/j.nanoen.2017.05.027>.
- [17] G. Cheng, Z.-H. Lin, Z. Du, Z.L. Wang, Increase output energy and operation frequency of a triboelectric nanogenerator by two grounded electrodes approach, *Adv. Funct. Mater.* 24 (2014) 2892–2898, <http://dx.doi.org/10.1002/adfm.201303659>.
- [18] X. Cheng, L. Miao, Y. Song, Z. Su, H. Chen, X. Chen, J. Zhang, H. Zhang, High efficiency power management and charge boosting strategy for a triboelectric nanogenerator, *Nano Energy* 38 (2017) 438–446, <http://dx.doi.org/10.1016/j.nanoen.2017.05.063>.
- [19] Simiao Niu, Ying Liu, Yu. Sheng Zhou, Sihong Wang, Long Lin, Zhong Lin Wang, Optimization of triboelectric nanogenerator charging systems for efficient energy harvesting and storage, *IEEE Trans. Electron Devices* 62 (2015) 641–647, <http://dx.doi.org/10.1109/TEDE.2014.2377728>.
- [20] Y. Zi, J. Wang, S. Wang, S. Li, Z. Wen, H. Guo, Z.L. Wang, Effective energy storage from a triboelectric nanogenerator, *Nat. Commun.* 7 (2016) 10987, <http://dx.doi.org/10.1038/ncomms10987>.
- [21] A.C.M. de Queiroz, Electrostatic vibrational energy harvesting using a variation of Bennet's doubler, *IEEE* (2010) 404–407, <http://dx.doi.org/10.1109/MWSCAS.2010.5548752>.
- [22] V. Dorzhiev, A. Karami, P. Basset, F. Marty, V. Dragunov, D. Galayko, Electret-free micromachined silicon electrostatic vibration energy harvester with the bennet's doubler as conditioning circuit, *IEEE Electron Device Lett.* 36 (2015) 183–185, <http://dx.doi.org/10.1109/LED.2014.2387213>.
- [23] E. Lefeuvre, S. Rissquez, J. Wei, M. Woytasik, F. Parrain, Self-biased inductor-less interface circuit for electret-free electrostatic energy harvesters, *J. Phys. Conf. Ser.* 557 (2014) 012052, <http://dx.doi.org/10.1088/1742-6596/557/1/012052>.
- [24] A. Ghaffarinejad, Y. Lu, R. Hinchet, D. Galayko, J.Y. Hasani, S.W. Kim, P. Basset, Bennet's doubler working as a power booster for triboelectric nano-generators, *Electron. Lett.* (2017), <http://dx.doi.org/10.1049/el.2017.3434>.
- [25] U.G. Musa, S.D. Cezan, B. Baytekin, H.T. Baytekin, The charging events in contact-separation electrification, *Sci. Rep.* 8 (2018), <http://dx.doi.org/10.1038/s41598-018-20413-1>.
- [26] J. Yao, F. Zhou, H. Yin, Y. Zhao, Q. Guo, N. Li, Experimental investigation of electrostatic charge generation for granules, *Procedia Eng.* 102 (2015) 287–294, <http://dx.doi.org/10.1016/j.proeng.2015.01.145>.
- [27] O.D. Jefimenko, D.K. Walker, Electrostatic current generator having a disk electret as an active element, *IEEE Trans. Ind. Appl. IA* 14 (1978) 537–540, <http://dx.doi.org/10.1109/TIA.1978.4503588>.
- [28] Y. Tada, Experimental characteristics of electret generator, using polymer film electrets, *Jpn. J. Appl. Phys.* 31 (1992) 846–851, <http://dx.doi.org/10.1143/JJAP.31.846>.
- [29] G.M. Sessler (Ed.), *Electrets*, Springer Berlin Heidelberg, Berlin, Heidelberg, 1987, <http://dx.doi.org/10.1007/3-540-17335-8>.
- [30] P. Keith Watson, Z.-Z. Yu, The contact electrification of polymers and the depth of charge penetration, *J. Electrostat.* 40–41 (1997) 67–72, [http://dx.doi.org/10.1016/S0304-3886\(97\)00016-8](http://dx.doi.org/10.1016/S0304-3886(97)00016-8).
- [31] A. Bennet, An account of a doubler of electricity, *Philos. Trans. LXXVII* (1787) 288–296.
- [32] A.C.M. de Queiroz, M. Domingues, The doubler of electricity used as battery charger, *IEEE Trans. Circuits Syst. II Express Briefs* 58 (2011) 797–801, <http://dx.doi.org/10.1109/TCSII.2011.2173963>.
- [33] A. Karami, D. Galayko, P. Basset, Series-parallel charge pump conditioning circuits for electrostatic kinetic energy harvesting, *IEEE Trans. Circuits Syst. Regul. Pap.* 64 (2017) 227–240, <http://dx.doi.org/10.1109/TCSI.2016.2603064>.
- [34] A. Ghaffarinejad, Y. Lu, R. Hinchet, D. Galayko, J.Y. Hasani, S.W. Kim, P. Basset, Bennet's doubler working as a power booster for triboelectric nano-generators, *Electron. Lett.* 54 (2018) 378–379, <http://dx.doi.org/10.1049/el.2017.3434>.
- [35] D. Galayko, A. Dudka, A. Karami, E. O'Riordan, E. Blokhina, O. Feely, P. Basset, Capacitive energy conversion with circuits implementing a rectangular charge-voltage cycle—Part 1: analysis of the electrical domain, *IEEE Trans. Circuits Syst. Regul. Pap.* 62 (2015) 2652–2663, <http://dx.doi.org/10.1109/TCSI.2015.2451911>.
- [36] E. Lefeuvre, S. Rissquez, J. Wei, M. Woytasik, F. Parrain, Self-biased inductor-less interface circuit for electret-free electrostatic energy harvesters, *J. Phys. Conf. Ser.* 557 (2014) 012052, <http://dx.doi.org/10.1088/1742-6596/557/1/012052>.
- [37] S. Wang, S. Niu, J. Yang, L. Lin, Z.L. Wang, Quantitative measurements of vibration amplitude using a contact-mode freestanding triboelectric nanogenerator, *ACS Nano* 8 (2014) 12004–12013, <http://dx.doi.org/10.1021/nm5054365>.
- [38] S. Wang, Y. Xie, S. Niu, L. Lin, Z.L. Wang, Freestanding triboelectric-layer-based nanogenerators for harvesting energy from a moving object or human motion in contact and non-contact modes, *Adv. Mater.* 26 (2014) 2818–2824, <http://dx.doi.org/10.1002/adma.201305303>.
- [39] E. O'Riordan, A. Dudka, D. Galayko, P. Basset, O. Feely, E. Blokhina, Capacitive energy conversion with circuits implementing a rectangular charge-voltage cycle Part 2: electromechanical and nonlinear analysis, *IEEE Trans. Circuits Syst. Regul. Pap.* 62 (2015) 2664–2673, <http://dx.doi.org/10.1109/TCSI.2015.2451913>.
- [40] A. Karami, D. Galayko, M. Bedier, P. Basset, Analysis and comparison of charge-pump conditioning circuits for capacitive electromechanical energy conversion, *IEEE* (2017) 1–4, <http://dx.doi.org/10.1109/ISCAS.2017.8050650>.
- [41] Goodfellow Inc, Wholesale and distribution company, website: <http://www.goodfellow.com/>, (n.d.).
- [42] Y. Lu, E. O'Riordan, F. Cottone, S. Boisseau, D. Galayko, E. Blokhina, F. Marty, P. Basset, A batch-fabricated electret-biased wideband MEMS vibration energy harvester with frequency-up conversion behavior powering a UHF wireless sensor node, *J. Micromech. Microeng.* 26 (2016) 124004, <http://dx.doi.org/10.1088/0960-1317/26/12/124004>.
- [43] Y. Lu, E. O'Riordan, F. Cottone, S. Boisseau, D. Galayko, E. Blokhina, F. Marty, P. Basset, A batch-fabricated electret-biased wideband MEMS vibration energy harvester with frequency-up conversion behavior powering a UHF wireless sensor node, *J. Micromech. Microeng.* 26 (2016) 124004, <http://dx.doi.org/10.1088/0960-1317/26/12/124004>.
- [44] R. Khambuya, S. Khwan-on, A new high step-down DC-DC converter for renewable energy system applications, *Procedia Comput. Sci.* 86 (2016) 349–352, <http://dx.doi.org/10.1016/j.procs.2016.05.094>.
- [45] S. Niu, X. Wang, F. Yi, Y.S. Zhou, Z.L. Wang, A universal self-charging system driven by random biomechanical energy for sustainable operation of mobile electronics, *Nat. Commun.* 6 (2015), <http://dx.doi.org/10.1038/ncomms9975>.
- [46] I. Park, J. Maeng, D. Lim, M. Shim, J. Jeong, C. Kim, A 4.5-to-16 μ W integrated triboelectric energy-harvesting system based on high-voltage dual-input buck converter with MPPT and 70V maximum input voltage, *IEEE* (2018) 146–148, <http://dx.doi.org/10.1109/ISSCC.2018.8310226>.
- [47] K.I. Hwu, W.Z. Jiang, Y.T. Yau, Ultrahigh step-down converter, *IEEE Trans. Power Electron.* 30 (2015) 3262–3274, <http://dx.doi.org/10.1109/TPEL.2014.2338080>.
- [48] M. Bedier, A. Karami, D. Galayko, P. Basset, Autonomous energy management interface for electrostatic series-parallel charge pump vibrational energy harvester, *IEEE* (2017) 385–388, <http://dx.doi.org/10.1109/NEWCAS.2017.8010186>.
- [49] Z. Chen, W. Tian, X. Zhang, Effect of surface asperities on the capacitances of capacitive RF MEMS switches, *J. Micromech. Microeng.* 27 (2017) 034002, <http://dx.doi.org/10.1088/1361-6439/aa5bb8>.
- [50] Z. Chen, W. Tian, X. Zhang, Y. Wang, Effect of deposition parameters on surface roughness and consequent electromagnetic performance of capacitive RF MEMS switches: a review, *J. Micromech. Microeng.* 27 (2017) 113003, <http://dx.doi.org/10.1088/1361-6439/aa8917>.
- [51] A. Ghaffari Nejad, J. Yavand Hasani, Effects of contact roughness and trapped free space on characteristics of RF-MEMS capacitive shunt switches, *Can. J. Electr. Comput. Eng.* 39 (2016) 132–140, <http://dx.doi.org/10.1109/CJECE.2015.2510700>.
- [52] J.B. Muldavin, G.M. Rebeiz, High-isolation CPW MEMS shunt switches. 1. Modeling, *IEEE Trans. Microw. Theory Tech.* 48 (2000) 1045–1052, <http://dx.doi.org/10.1109/22.904743>.
- [53] Y. Zi, S. Niu, J. Wang, Z. Wen, W. Tang, Z.L. Wang, Standards and figure-of-merits for quantifying the performance of triboelectric nanogenerators, *Nat. Commun.* 6 (2015), <http://dx.doi.org/10.1038/ncomms9376>.
- [54] http://www.datasheetarchive.com/files/spicemodels/misc/modelos/spice_complete/fairch.lib, (n.d.).



Ali Ghaffarinejad is pursuing his Ph.D. degree under supervision of Professor Javad Yavand Hasani at School of Electrical Engineering, Iran University of Science and Technology (IUST), Tehran, Iran. He is currently a visiting student at ESYCOM lab, Université Paris-Est/ESIEE, Paris, France. He received his B.Sc. degree in Electronic engineering from the University of Kerman, Iran, in 2006, the M.Sc. degree in Bioelectronics from IUST in 2011. His research interests include modeling of triboelectric charge generation and stability in kinetic energy harvesters and RF-MEMS devices. Currently he is focusing on power management circuits for triboelectric-electret energy harvesters.



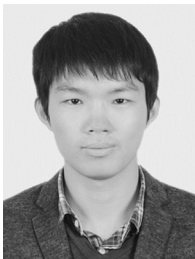
Javad Yavand Hasani is a professor in the School of Electrical Engineering at Iran University of Science and Technology (IUST), Tehran, Iran. In 2009 he received the PhD degree in electrical engineering from the University of Tehran and the PhD degree in high frequency and optics from the University of Joseph Fourier (UJF), Grenoble, France. From 2012–2014 he was the dean of the Electronic Research Center (ERC) in IUST. His current research interests include high frequency circuits and systems, as well as micro-fabrication theory and technology for RF and microwave devices, MEMS and NEMS.



Ronan Hinchet is a postdoctoral researcher in the School of Advanced Materials Science and Engineering at Sungkyunkwan University (SKKU). He received his PhD degree from the University of Grenoble in Nanoelectronics and Nanotechnology in 2014. His research interests are the simulation, fabrication, and characterization of nanostructures and nanomaterials for micro-electro-mechanical system and nano-electro-mechanical system applications. His research is focused on mechanical energy harvesters and mechanical sensor applications.



Yingxian Lu is a PhD student under the co-supervision of Professor Philippe Basset and Jean-Marc Laheurte at ESYCOM lab, Université Paris-Est. Her research interests include kinetic energy harvesters for power supply applications of wireless sensor nodes or for wearable electronics, MEMS device modeling, design and characterization, RF system optimization, and flexible electronic devices. Her research is focused on capacitive kinetic energy harvesters working with ultra-low frequency vibrations or motions, including random environmental vibrations, machine vibrations, or human motions.



Hemin Zhang received his B. Eng degree from Department of Electrical Engineering and Automation in 2011, and the Ph.D. degree from the MOE Key Laboratory of Micro and Nano Systems for Aerospace in 2017, both in Northwestern Polytechnical University, Xi'an, China. He is currently a postdoc in Université Paris-Est, ESYCOM Lab., ESIEE Paris. His research interests include mode-localized resonant MEMS sensors and triboelectric nanogenerator. He was a recipient of the Transducer 2015 Outstanding Paper Finalist Award and the MEMS 2016 Outstanding Paper Award.



Armine Karami was born in Paris, France, in 1991. He received the BSc and MSc degrees in electrical engineering from Sorbonne Université (formerly UPMC) in 2012 and 2014. He is currently pursuing a PhD degree in at Sorbonne Université, Paris, at the Laboratoire d'Informatique de Paris 6 (LIP6). His PhD research is focused on the theory and analysis of electrostatic kinetic energy harvesting systems.



Dimitri Galayko was graduated from Odessa State Polytechnic University (Ukraine) in 1998, he received his master degree from Institute of Applied Sciences of Lyon (INSA-LYON, France) in 1999. He made his PhD thesis in the Institute of Microelectronics and Nanotechnologies (IEMN, Lille, France) and received the PhD degree from the University Lille-I in 2002. Since 2005 he is an associate professor in University Paris VI (UPMC, Sorbonne Universités) in the Laboratory of Computer Science (LIP6). His research interests cover design and modeling of heterogeneous systems involving a combination of classical CMOS integrated circuit with physical sensors such as MEMS devices and energy harvesters, study of different aspects of oscillating structures in microelectronics (both solid-state CMOS oscillators and MEMS oscillators), and investigation and modeling of nonlinear phenomena emerging in such systems. He is an active member of the Technical Committee Nonlinear Circuits and Systems of IEEE CAS society.



Sang-Woo Kim is a professor in the Department of Advanced Materials Science and Engineering at Sungkyunkwan University (SKKU). His recent research interest is focused on piezoelectric/triboelectric nanogenerators, sensors, and photovoltaics using nanomaterials. He has published over 200 peer-reviewed papers and holds over 80 domestic/international patents. Now he is a director of SAMSUNG-SKKU Graphene/2D Research Center and is leading National Research Laboratory for Next Generation Hybrid Energy Harvester. He is currently serving as an Associate Editor of *Nano Energy* and an Executive Board Member of *Advanced Electronic Materials*.



Philippe Basset received his Ph.D from IEMN, University of Lille in 2003 in the areas of microelectronic and micro-electro-mechanical-systems (MEMS). In 2004 he was a post-doc at CMU, Pittsburgh, USA and he joined ESIEE Paris in 2005 where he is associate professor. His current research interests include micro-power sources for autonomous systems and micro/nano-structuration of silicon. He serves in the International Steering Committee of the PowerMEMS conference since 2015 and is currently deputy director of the ESYCOM laboratory.